GEOPHYSICS

10.1126/sciadv.1400260

Unraveling the complexity of iron oxides at high pressure and temperature: Synthesis of Fe_5O_6

Barbara Lavina[1]* and Yue Meng[2]

The iron-oxygen system is the most important reference of rocks' redox state. Even as minor components, iron oxides can play a critical role in redox equilibria, which affect the speciation of the fluid phases chemical differentiation, melting, and physical properties. Until our recent finding of Fe_4O_5, iron oxides were assumed to comprise only the polymorphs of FeO, Fe_3O_4, and Fe_2O_3. Combining synthesis at high pressure and temperature with microdiffraction mapping, we have identified yet another distinct iron oxide, Fe_5O_6. The new compound, which has an orthorhombic structure, was obtained in the pressure range from 10 to 20 GPa upon laser heating mixtures of iron and hematite at ~2000 K, and is recoverable to ambient conditions. The high-pressure orthorhombic iron oxides Fe_5O_6, Fe_4O_5, and *h*-Fe_3O_4 display similar iron coordination geometries and structural arrangements, and indeed exhibit coherent systematic behavior of crystallographic parameters and compressibility. Fe_5O_6, along with FeO and Fe_4O_5, is a candidate key minor phase of planetary interiors; as such, it is of major petrological and geochemical importance. We are revealing an unforeseen complexity in the Fe-O system with four different compounds—FeO, Fe_5O_6, Fe_4O_5, and *h*-Fe_3O_4—in a narrow compositional range (0.75 < Fe/O < 1.0). New, finely spaced oxygen buffers at conditions of the Earth's mantle can be defined.

INTRODUCTION

Iron and oxygen are two of the most abundant elements of terrestrial planets. Participating in redox equilibria and carrying magnetism, the petrological and geochemical significance of iron oxides far exceeds their abundance (*1*). Extreme conditions control planetary interior processes and dynamics, as well as the outcome of large impacts on planets' surfaces. Thus, it is fundamental to define structures, stability, properties, and crystal chemistry of iron oxides at high pressure and temperature.

The recent discovery of the high-pressure compound Fe_4O_5 (*2*) demonstrates that our understanding of one of the binary systems most important for the evolution of terrestrial planets is far too limited. The implied assumption that only the polymorphism of previously known iron oxides should be determined has been proven to limit our perspectives on planetary modeling. Fe_4O_5 has a layered structure stable at pressures greater than 10 GPa (*2*) and up to at least 40 GPa (*3*). Compositionally, its stability range extends toward high oxygen contents, because Fe_3O_4 was observed to break down into Fe_4O_5 and hematite at about 10 GPa (*4*). Furthermore, Fe_4O_5 has been found to accept large amounts of isomorphous substitutions (*5*). There is a clear parallelism between the structures of high-pressure orthorhombic iron oxides and those of calcium ferrites. Fe_4O_5 adopts the same structure of $CaFe_3O_5$ (*2*), whereas *h*-Fe_3O_4 assumes the arrangement of $CaTi_2O_4$, which is similar to the structure of $CaFe_2O_4$. On the basis of this systematics, we speculated that a new iron oxide might be stable at high pressure, a compound analogous to $CaFe_4O_6$ (*6*). We thereby investigated the FeO system at compositions close to Fe/O = 0.83 at high pressure and temperature, adopting advanced structural analysis techniques. Here, we report the discovery of a new compound, Fe_5O_6.

[1]High Pressure Science and Engineering Center, University of Nevada, Las Vegas, Las Vegas, NV 89154–4002, USA. [2]High Pressure Collaborative Access Team, Carnegie Institution of Washington, Argonne, IL 60439–4803, USA.
*Corresponding author. E-mail: lavina@physics.unlv.edu

RESULTS

Mixtures of iron and hematite ($Fe + 2Fe_2O_3 \rightarrow Fe_5O_6$) were pressurized to targeted pressure values (10 to 20 GPa) and subsequently heated up to ~2300 K using the online double-sided infrared (IR) laser heating technique (*7*). The samples, roughly 80 to 200 μm in diameter and 10 μm in thickness, were translated in front of the laser beams to convert most of the starting material into high-pressure products. The reaction progress was monitored by collecting diffraction patterns every ~30 s during the heating. The conversion of iron and hematite mixtures to high-pressure forms of oxides is prompt and complete upon achieving homogeneous heating. We heated some samples for up to 30 minutes and did not observe further phase changes. The high-pressure phases show unstrained diffraction peaks and grain size growth as shown by the spotty Debye rings in fig. S1. These observations suggest that the reactions proceeded toward definite lower energetic minima. There is no evidence of dissociation reactions or phase transitions upon temperature quenching (figs. S2 and S3).

After the synthesis, samples typically display heterogeneity with respect to phase and grain size distributions. Heterogeneities are a consequence of thermally induced chemical gradients and the narrow compositional differences between high-pressure orthorhombic iron oxides. Diffraction data were collected in fine two-dimensional grids before and after laser heating at high pressure for proper characterization of synthesis products. The microdiffraction mapping (*8*) allowed us to identify all phases, find the locations most suitable for the crystallographic analysis of each phase, and map the phase distribution. In most patterns, we observed diffraction peaks that could not be attributed to any of the known iron oxides. Considering that the interpretation of multiphase powder diffraction data is often non-unique, particularly when coexisting phases have relatively large and comparable unit cell parameters, we performed multiple syntheses and purposely searched for micrometer-sized crystal grains. Therefore, our structural determination is based on the larger grains for which the diffraction effects could be isolated in the three dimensions of the reciprocal space.

The structure of the unknown phase was determined from the diffraction effects of a few selected grains isolated in multiphase diffraction images, an example of which is shown in Fig. 1A. This approach ensures unique index assignment (Fig. 1B). The peaks were indexed with an orthorhombic unit cell, with parameters a = 2.815(10) Å, b = 9.795(3) Å, and c = 15.011(4) Å at 11.4 GPa, 300 K. The cell parameters a and b are comparable to those of Fe_4O_5 and h-Fe_3O_4. The length of c is about 3 Å greater than that in Fe_4O_5, roughly the same difference observed between Fe_4O_5 and h-Fe_3O_4 (fig. S4). It follows that the unit cell volume of the new phase is ~150 $Å^3$ larger than that of Fe_4O_5, a difference similar to that observed between Fe_4O_5 and h-Fe_3O_4 (fig. S5). The unit cell comparison provided the first evidence that the stoichiometry of the phase could indeed be that of the new compound Fe_5O_6. We therefore proceeded with the analysis of observed structure factors and obtained the space group *Cmcm* as the most plausible symmetry. Refinements with the structural model of $CaFe_4O_6$ resulted in substantial agreement between the observed and calculated structure factors of multiple grains from different samples. An example of a structural refinement obtained for a grain synthesized at 11.4 GPa is shown in Table 1.

In the structure of Fe_5O_6, iron is located in three non-equivalent crystallographic sites with point group symmetries *4c*, *8f*, and *8f* (Fig. 2). Like the other high-pressure orthorhombic iron oxides, Fe_5O_6 has a layered structure where edge-sharing FeO_6 octahedra alternate with FeO_6 trigonal prisms perpendicularly to the c axis. The layers of octahedra are two, three, and four atoms thick for h-Fe_3O_4, Fe_4O_5, and Fe_5O_6, respectively. The relation in structural arrangements in the series of high-pressure iron oxides is consistent with the aforementioned trends in unit cell parameter lengths (fig. S4). The a unit cell parameters of Fe_4O_5 and Fe_5O_6 are similar in the investigated pressure range, whereas the b parameters differ by roughly 0.15 Å (fig. S4). Considering that the shortest Fe-Fe distances (=a) occur between equivalent iron atoms in the direction parallel to the a axis, the a cell parameter might be controlled by the Fe-Fe repulsion and therefore the charge distribution between iron sites. The b axis length is, in the first approximation, controlled by the size of the octahedra. The average charge of iron in Fe_5O_6 is lower than that in Fe_4O_5, which translates to a greater mean octahedral size, and may explain the difference in b axis lengths of the two phases (fig. S4). The largest average Fe–O bonds were observed for iron in the trigonal prismatic coordination, similarly to what has been observed in Fe_4O_5 (*2*). The two octahedra appear to differ significantly in size and degree of distortion (Table 1). The Fe1 octahedron (dark blue in Fig. 2) is smaller and less distorted than the Fe2 octahedron (light blue in Fig. 2).

The phase maps in Fig. 3 illustrate an example of the spatial distribution of the synthesis products. Fe_5O_6 is abundant in the space separating regions high in wüstite and in Fe_4O_5, corroborating the composition proposed for the new compound, which is intermediate between the two known phases. Although we do not exclude the existence

Table 1. Structural data of Fe_5O_6 at 11.4 GPa. The least-squares refinement of the unit cell parameters was performed against 200 reflections. The refinement of 10 atomic fractional coordinates and the scale factor was performed against 81 F_o^2 (after averaging symmetry equivalents), and converged with satisfactory statistical parameters ($R_{4\sigma}$ = 10%, R_{all} = 11%).

P (GPa)	11.4
T (K)	300
K_0 (GPa)	173(2)
a (Å)	2.815(10)
b (Å)	9.795(3)
c (Å)	15.011(4)
V ($Å^3$)	414(2)
<Fe_{4c}-O> (Å)	2.076
<Fe_{8f1}-O> (Å)	2.058
<Fe_{8f2}-O> (Å)	2.075
x, y, z (Fe_{4c})	0, 0.6379(5), ¼
x, y, z (Fe_{8f1})	0, 0.1341(3), 0.4527(3)
x, y, z (Fe_{8f2})	0, 0.3959(4), 0.3568(4)
x, y, z (O1)	0, 0.290(2), ¼
x, y, z (O2)	0, 0.782(2), 0.421(2)
x, y, z (O3)	0, 0.043(2), 0.332(2)
x, y, z (O4)	0, ½, 0

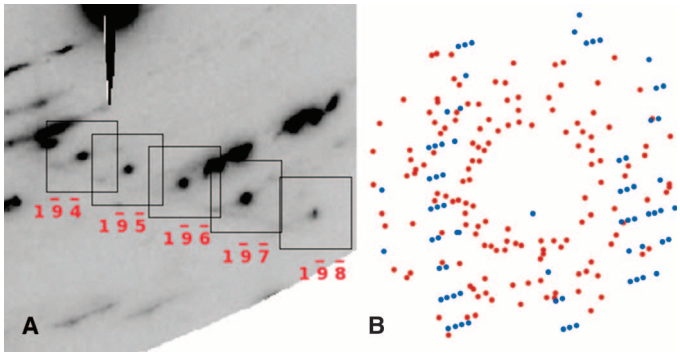

Fig. 1. Row of reflections of an Fe_5O_6 crystal in a multiphase diffraction pattern. (**A**) Detail of an x-ray diffraction pattern collected at 18 GPa, highlighting an indexed row of peaks belonging to an Fe_5O_6 crystal. (**B**) In a projection in the reciprocal space of all reflections, those belonging to the Fe_5O_6 grain are shown in blue.

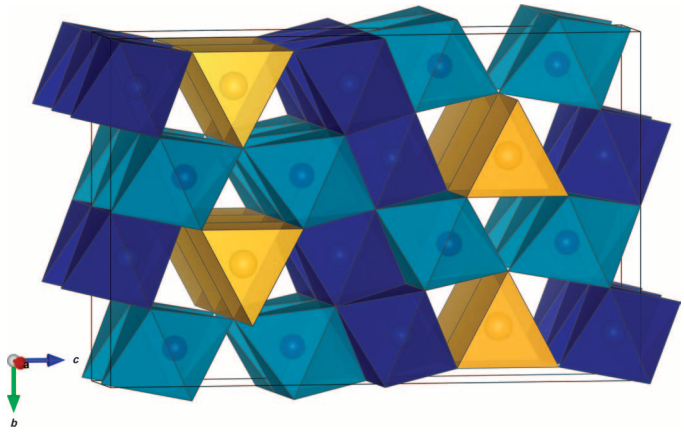

Fig. 2. The structure of Fe_5O_6. The trigonal prisms representing the coordination environment of iron in the *4c* position are shown in yellow. Layers of edge-sharing coordination octahedra of iron in the *8f* positions are shown in two shades of blue representing two non-equivalent crystallographic sites.

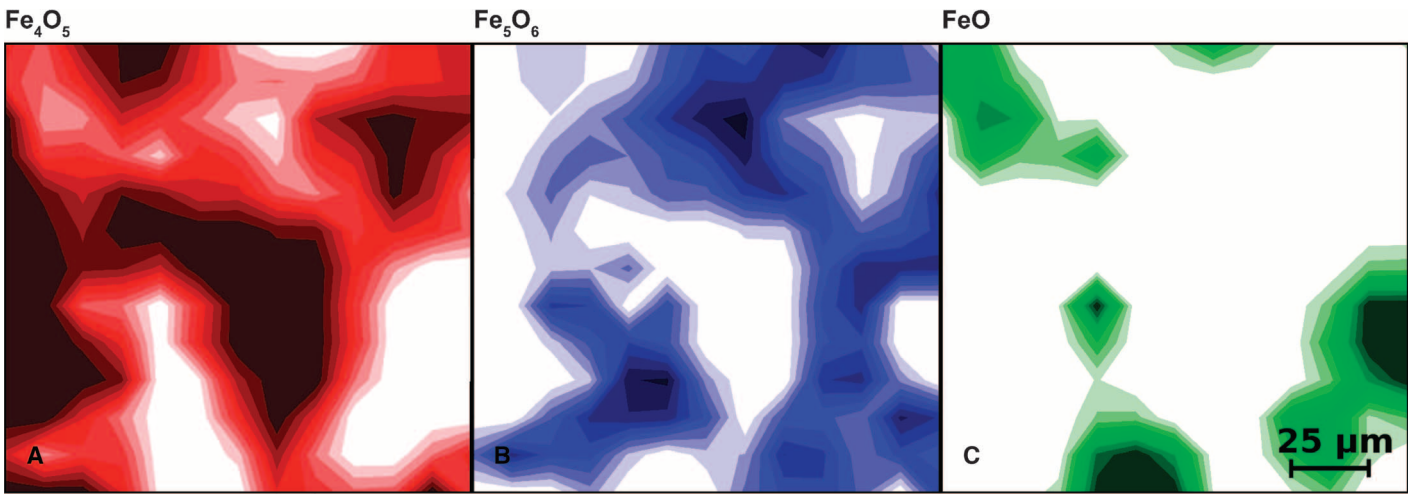

Fig. 3. Compositional maps after high *P-T* synthesis. Distribution of the iron oxide phases identified after heating a mixture of hematite and iron at 11 GPa and up to about 2300 K. The maps represent the relative abundances of Fe_4O_5 (red), Fe_5O_6 (blue), and wüstite (green). Abundances from 0 to 100% are represented in 10 color shades; deeper colors correspond to higher concentrations. These maps were obtained from 13 × 13 data points and measure 150 μm in both the horizontal and vertical directions.

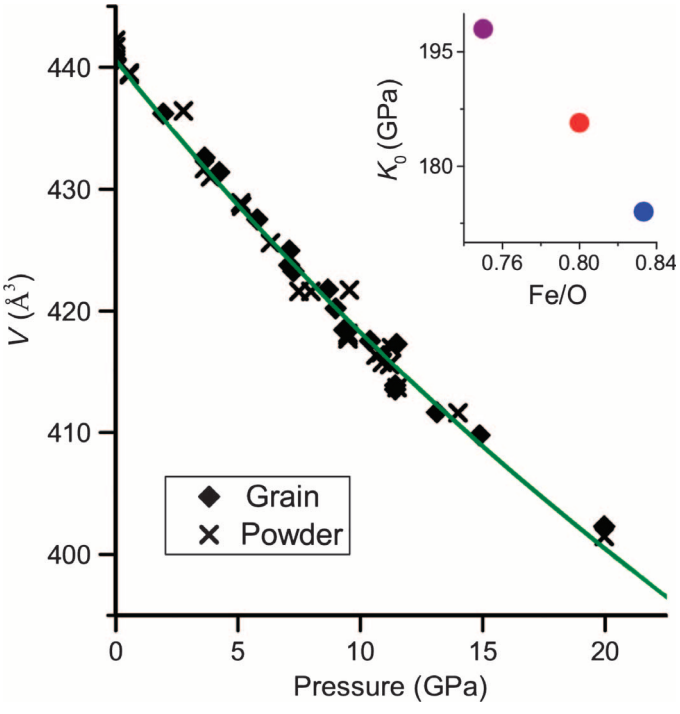

Fig. 4. Bulk compressibility of Fe_5O_6. Data obtained from the grain analysis are represented by solid symbols, and those from the multiphase powder diffraction patterns by crosses. The solid curve represents the fit of a second-order Birch-Murnaghan equation of state (see text). The inset shows the bulk modulus against composition of the three orthorhombic iron oxides *h*-Fe_3O_4 (purple), Fe_4O_5 (red), and Fe_5O_6 (blue). SD values are smaller than the symbol sizes.

of even more complex iron oxides (with formula Fe_5O_6 + *n*FeO), we do not have clear evidence of other phases compositionally intermediate between Fe_5O_6 and wüstite within the investigated pressure and temperature ranges.

We found that Fe_5O_6, like Fe_4O_5, is recoverable, whereas *h*-Fe_3O_4 reverts to magnetite at pressures lower than 5 GPa (*9*). The bulk compressibility of Fe_5O_6 is shown in Fig. 4; our measured ambient condition volume is 440.6 (5) Å^3. The bulk modulus of Fe_5O_6, estimated by fitting the data to the second-order Birch-Murnaghan equation of state, is 173 (2) GPa. Fe_5O_6 is, expectedly, more compressible than Fe_4O_5 [K_0 = 185.7 GPa (2)] and *h*-Fe_3O_4 [K_0 = 198 GPa (*10*)]. The bulk moduli of the three orthorhombic iron oxides follow a Vegard's trend (Fig. 4, inset), further supporting the inferred composition.

DISCUSSION

The oxygen fugacity of the Earth's mantle varies in three dimensions as a result of the crystal chemical control of major phases, the raise of reduced material from the bottom regions of the mantle, and the incorporation of oxidized materials from subduction [for example, (*11*–*13*)]. Redox equilibria influence phase stability and properties, differentiation and melting, and ultimately have a strong role in the whole planetary chemical and physical dynamics. All phases containing elements with multiple valence states participate in redox equilibria, chiefly the most abundant iron-bearing silicates and magnesiowüstite [for example, (*13*–*15*)]. Nonetheless, minor iron-bearing phases, such as iron oxides, can play a critical role in mantle redox equilibria (*16*), particularly in locally iron-rich environments.

Fe_5O_6 is a new high-pressure iron oxide that was characterized by high-pressure microdiffraction analysis and is supported by the consistent behavior of structural parameters and compressibility in the series of orthorhombic high-pressure iron oxides. The synthesis is rapid and repeatable, with no evidence of further structural transitions upon temperature quenching and pressure release. The spatial distribution of coexisting iron oxides in several samples synthesized at high pressure and temperature supports the composition inferred for the new compound. The samples did not reach chemical homogeneity; we found that wüstite, Fe_5O_6, and Fe_4O_5 are stable at the same pressure and temperature, and their distribution follows

chemical gradients. Fe_5O_6 and Fe_4O_5 are fairly reduced and therefore likely to occur in planetary interiors as modally minor components. Different oxides close in composition might be stabilized as a result of modest differences in oxygen fugacity. Wüstite, in association with ferrite, has been observed in superdeep diamond inclusions (*17*), a direct evidence that such phases can exist in the Earth's mantle. The iron-oxygen system has a petrologic significance far exceeding the abundance of its phases. Equilibria in the Fe-O system constitute the most important oxygen buffers [iron-wüstite (IW), magnetite-wüstite (MW), and magnetite-hematite (MH); for example, (*18*)] and are indeed the reference of oxygen fugacity of rocks. Phase stability with respect to oxidation state is indeed typically defined relative to redox exchanges with iron oxides [for example, (*19*–*27*)]. At pressure greater than 10 GPa, we have found that the iron-oxygen system is surprisingly complex, Fe_5O_6 being the fourth compound described in a narrow compositional range, between 0.75 and 1.0 Fe/O, in addition to FeO, Fe_4O_5, and Fe_3O_4. With the discovery of Fe_5O_6 and Fe_4O_5, we can define new, finely spaced oxygen fugacity buffers that apply to pressures greater than ~10 GPa. These are given by the reactions $5FeO + 1/2\ O_2 = Fe_5O_6$; $4FeO + 1/2\ O_2 = Fe_4O_5$, and $3Fe_4O_5 + 1/2\ O_2 = 4\ Fe_3O_4$. Fe_5O_6 and Fe_4O_5 are plausible new players in the Earth's mantle redox equilibria. Assessing the degree of the influence of these phases on planetary interior processes is a challenging task that requires the petrological analysis of complex systems of realistic compositions.

High-resolution structural studies at extreme conditions allow unraveling the complexity of matter at high pressure, as we have shown here for the binary system of the Earth's two most abundant elements. Concurrently, enhanced resolution of seismic profiles reveals the marked heterogeneities in the Earth's mantle. Parallel paradigm shifts that span from mantle lateral heterogeneity to the Fe-O system high-pressure behavior might be related by an unforeseen complexity of redox equilibria.

MATERIALS AND METHODS

Iron and hematite fine powders were mixed in appropriate proportions ($Fe + 2F_2O_3 = Fe_5O_6$) and loaded at pressures ranging from ~10 to ~20 GPa in diamond anvil cells. Neon was used as pressure medium and thermal insulator for laser heating under high pressures, whereas gold and ruby were used as pressure standards. The samples, pressurized between 10 and 20 GPa, were heated to temperatures of about 2000 K using a double-sided IR laser heating system (*7*) installed in the 16IDB experimental station of the High Pressure Collaborative Access Team (HPCAT), Advanced Photon Source (APS), Argonne National Laboratory. We used a relatively large heating spot size, about 30 μm in flat top area and 60 μm in full width at half maximum (FWHM), at the same time, moving the sample position relative to the heating laser to ensure the conversion of the whole sample into the high-pressure phases of iron oxides. Although the synthesis is fast, we heated the samples for ~15 min, moving the cells and adjusting the laser power to complete the reaction of the whole sample. Monochromatic hard x-ray beams of energy ranging between 30 and 37 keV focused to 6 × 5–μm FWHM were used for the structural characterization. Even with such a small beam, only a few diffraction images collected were single-phase Fe_5O_6, and they were typically neither ideal powder nor single-crystal patterns. The grain size of the samples appears to be fairly coarse and highly variable. The finer-textured diffraction patterns were processed with powder diffraction methods and used for lattice parameter determination (table S1). None of these powder patterns were suitable for a reliable structure analysis of Fe_5O_6 atomic parameters. Diffraction intensities were nonetheless used for the rough determination of phase abundances. A few locations, identified while microdiffraction mapping the samples, showed relatively large grains of Fe_5O_6 with low strain in multiphase diffraction images. The diffraction peaks of these grains, isolated in the reciprocal space, provide conclusive determination of the structure of Fe_5O_6. Pressure-dependent data were collected in decompression, assuring a quasi-hydrostatic stress field. The softwares GSE_ADA, RSV (*28*), SHELXL (*29*), FIT2D (*30*), and Jade were used for reduction and refinement of diffraction data. VESTA (*31*) was used for the representation of the structure. The nominal composition of these phases is deduced from the structural analysis of single crystal grains; minor differences in stoichiometry cannot be discriminated with this approach.

SUPPLEMENTARY MATERIALS

Supplementary material for this article is available at http://advances.sciencemag.org/cgi/content/full/1/5/e1400260/DC1

Fig. S1. Diffraction image (**A**) and integrated pattern (**B**) collected during synthesis (~15 GPa, ~2000 K).

Fig. S2. Diffraction image (**A**) and integrated pattern (**B**) collected at 10.7 GPa where Fe_5O_6, wüstite, neon, and gold were the phases identified.

Fig. S3. Diffraction image (**A**) and integrated pattern (**B**) collected at ~11 GPa where Fe_5O_6, Fe_4O_5, and neon were the phases identified.

Fig. S4. Comparison of the axial compressibility of Fe_5O_6 and Fe_4O_5.

Fig. S5. Volume (**A**) and relative compressibility (**B**) of the orthorhombic iron oxides.

Table S1. Example of cell parameter fitting results from powder diffraction analysis.

References (*32*–*34*)

REFERENCES AND NOTES

1. B. R. Frost, Introduction to oxygen fugacity and its petrologic importance. *Rev. Mineral. Geochem.* **25**, 1–9 (1991).
2. B. Lavina, P. Dera, E. Kim, Y. Meng, R. T. Downs, P. F. Weck, S. R. Sutton, Y. Zhao, Discovery of the recoverable high-pressure iron oxide Fe_4O_5. *Proc. Natl. Acad. Sci. U.S.A.* **108**, 17281–17285 (2011).
3. K. Kothapalli, E. Kim, T. Kolodziej, P. F. Weck, E. E. Alp, Y. Xiao, P. Chow, C. Kenney-Benson, Y. Meng, S. Tkachev, A. Kozlowski, B. Lavina, Y. Zhao, Nuclear forward scattering and first-principles studies of the iron oxide phase Fe_4O_5. *Phys. Rev. B* **90**, 024430 (2014).
4. A. B. Woodland, D. J. Frost, D. M. Trots, K. Klimm, M. Mezouar, In situ observation of the breakdown of magnetite (Fe_3O_4) to Fe_4O_5 and hematite at high pressures and temperatures. *Am. Mineral.* **97**, 1808–1811 (2012).
5. A. B. Woodland, K. Schollenbruch, M. Koch, T. B. Ballaran, R. J. Angel, D. J. Frost, Fe_4O_5 and its solid solutions in several simple systems. *Contrib. Mineral. Petrol.* **166**, 1677–1686 (2013).
6. O. Evrard, B. Malaman, F. Jeannot, A. Courtois, H. Alebouyeh, R. Gerardin, The synthesis of a new calcium ferrite ($CaFe_4O_6$) and determination of calcium-ferrite crystalline-structures $CaFe_{2+n}O_{4+n}$—A new example of the intergrowth process. *J. Solid State Chem.* **35**, 112–119 (1980).
7. Y. Meng, R. Hrubiak, E. Rod, R. Boehler, G. Shen, New developments in laser-heated diamond anvil cell with in-situ synchrotron x-ray diffraction at HPCAT. *Rev. Sci. Instrum.*, submitted (2015).
8. B. Lavina, P. Dera, Y. Meng, Synthesis and microdiffraction at extreme pressures and temperatures. *J. Vis. Exp.* e50613 (2013).
9. H. Mao, T. Takahash, W. Bassett, G. Kinsland, L. Merrill, Isothermal compression of magnetite to 320 kbar and pressure-induced phase-transformation. *J. Geophys. Res.* **79**, 1165–1170 (1974).
10. L. Dubrovinsky, N. Dubrovinskaia, C. McCammon, G. Rozenberg, R. Ahuja, J. Osorio-Guillen, V. Dmitriev, H. Weber, T. Le Bihan, B. Johansson, The structure of the metallic high-pressure Fe_3O_4 polymorph: Experimental and theoretical study. *J. Phys. Condens. Matter* **15**, 7697–7706 (2003).

11. B. Wood, L. Bryndzia, K. Johnson, Mantle oxidation-state and its relationship to tectonic environment and fluid speciation. *Science* **248**, 337–345 (1990).
12. D. Frost, C. Liebske, F. Langenhorst, C. McCammon, R. Trønnes, D. Rubie, Experimental evidence for the existence of iron-rich metal in the earth's lower mantle. *Nature* **428**, 409–412 (2004).
13. D. J. Frost, C. A. McCammon, The redox state of Earth's mantle. *Rev. Earth Planet. Sci.* **36**, 389–420 (2008).
14. V. Stagno, D. J. Frost, Carbon speciation in the asthenosphere: Experimental measurements of the redox conditions at which carbonate-bearing melts coexist with graphite or diamond in peridotite assemblages. *Earth Planet. Sci. Lett.* **300**, 72–84 (2010).
15. V. Stagno, D. O. Ojwang, C. A. McCammon, D. J. Frost, The oxidation state of the mantle and the extraction of carbon from Earth's interior. *Nature* **493**, 84–88 (2013).
16. C. McCammon, Microscopic properties to macroscopic behaviour: The influence of iron electronic state. *J. Mineral. Petrol. Sci.* **101**, 130–144 (2006).
17. R. Wirth, L. F. Dobrzhinetskaya, B. Harte, A. Schreiber, H. W. Green, High-Fe (Mg,Fe)O inclusion in diamond apparently from the lowermost mantle. *Earth Planet. Sci. Lett.* **404**, 365–375 (2014).
18. J. T. Myers, H. Eugster, The system Fe–Si–O: Oxygen buffer calibrations to 1,500K. *Contrib. Mineral. Petrol.* **82**, 75–90 (1983).
19. D. A. Hewitt, A redetermination of the fayalite–magnetite–quartz equilibrium between 650 degrees and 850 degrees C. *Am. J. Sci.* **278**, 715–724 (1978).
20. T. Yagi, T. Hishinuma, Iron hydride formed by the reaction of iron, silicate, and water: Implications for the light element of the Earth's core. *Geophys. Res. Lett.* **22**, 1933–1936 (1995).
21. E. Ohtani, N. Hirao, T. Kondo, M. Ito, T. Kikegawa, Iron-water reaction at high pressure and temperature, and hydrogen transport into the core. *Phys. Chem. Mineral.* **32**, 77–82 (2005).
22. B. Wood, A. Pawley, D. Frost, Water and carbon in the Earth's mantle. *Philos. Trans. A Math. Phys. Eng. Sci.* **354**, 1495–1511 (1996).
23. S. K. Saxena, H. P. Liermann, G. Y. Shen, Formation of iron hydride and high-magnetite at high pressure and temperature. *Phys. Earth Planet. Int.* **146**, 313–317 (2004).
24. H. Scott, R. Hemley, H. Mao, D. Herschbach, L. Fried, W. Howard, S. Bastea, Generation of methane in the earth's mantle: In situ high pressure–temperature measurements of carbonate reduction. *Proc. Natl. Acad. Sci. U.S.A.* **101**, 14023–14026 (2004).
25. M.Isshiki, T. Irifune, K. Hirose, S. Ono, Y. Ohishi, T. Watanuki, E. Nishibori, M. Takata, M. Sakata, Stability of magnesite and its high-pressure form in the lowermost mantle. *Nature* **427**, 60–63 (2004).
26. A. R. Oganov, S. Ono, Y. Ma, C. W. Glass, A. Garcia, Novel high-pressure structures of $MgCO_3$, $CaCO_3$ and CO_2 and their role in earth's lower mantle. *Earth Planet. Sci. Lett.* **273**, 38–47 (2008).
27. H. P. Scott, V. M. Doczy, M. R. Frank, M. Hasan, J.-F. Lin, J. Yang, Magnesite formation from MgO and CO_2 at the pressures and temperatures of Earth's mantle. *Am. Mineral.* **98**, 1211–1218 (2013).
28. P. Dera, K. Zhuravlev, V. Prakapenka, M. L. Rivers, G. J. Finkelstein, O. Grubor-Urosevic, O. Tschauner, S. M. Clark, R. T. Downs, High pressure single-crystal micro X-ray diffraction analysis with GSE_ADA/RSV software. *High Press. Res.* **33**, 466–484 (2013).
29. G. M. Sheldrick, A short history of SHELX. *Acta Cryst. A* **64**, 112–122 (2008).
30. A. Hammersley, S. Svensson, M. Hanfland, A. Fitch, D. Häusermann, Two-dimensional detector software: From real detector to idealised image or two-theta scan. *High Press. Res.* **14**, 235–248 (1996).
31. K. Momma, F. Izumi, *VESTA3* for three-dimensional visualization of crystal, volumetric and morphology data. *J. Appl. Cryst.* **44**, 1272–1276 (2011).
32. J. Guignard, W. A. Crichton, Synthesis and recovery of bulk Fe_4O_5 from magnetite, Fe_3O_4. A member of a self-similar series of structures for the lower mantle and transition zone. *Mineral. Mag.* **78**, 361–371 (2014).
33. Y. Fei, D. Frost, H. Mao, C. Prewitt, D. Hausermann, In situ structure determination of the high-pressure phase of Fe_3O_4. *Am. Mineral.* **84**, 203–206 (1999).
34. C. Haavik, S. Stolen, H. Fjellvag, M. Hanfland, D. Hausermann, Equation of state of magnetite and its high-pressure modification: Thermodynamics of the Fe-O system at high pressure. *Am. Mineral.* **85**, 514–523 (2000).

Acknowledgments: We are sincerely grateful to S. Tkachev for his assistance with the gas loadings. **Funding:** This research was sponsored by the National Nuclear Security Administration under the Stewardship Science Academic Alliances program through the U.S. Department of Energy (DOE) Cooperative Agreement DE-NA0001982. This work was conducted at HPCAT (Sector 16), APS, Argonne National Laboratory. HPCAT operations are supported by DOE–National Nuclear Security Administration under award no. DE-NA0001974 and DOE–Basic Energy Sciences (BES) under award no. DE-FG02-99ER45775, with partial instrumentation funding by the National Science Foundation (NSF). APS is supported by DOE-BES, under contract no. DE-AC02-06CH11357. Use of the COMPRES-GSECARS gas loading system was supported by COMPRES under NSF Cooperative Agreement EAR 11-57758 and by GSECARS through NSF grant EAR-1128799 and DOE grant DE-FG02-94ER14466. **Author contributions:** B.L. designed the study, collected and processed the data, and wrote the paper. Y.M. designed and built the experimental setup used for this study and contributed to the manuscript. **Competing interests:** The authors declare that they have no competing interests.

Submitted 25 December 2014
Accepted 22 April 2015
Published 26 June 2015
10.1126/sciadv.1400260

Citation: B. Lavina, Y. Meng, Unraveling the complexity of iron oxides at high pressure and temperature: Synthesis of Fe_5O_6. *Sci. Adv.* **1**, e1400260 (2015).

Science Advances

Unraveling the complexity of iron oxides at high pressure and temperature: Synthesis of Fe_5O_6

Barbara Lavina and Yue Meng

Sci Adv **1** (5), e1400260.
DOI: 10.1126/sciadv.1400260